LIMNOLOGY AND OCEANOGRAPHY
Letters

ASLO
Open Access

Limnology and Oceanography Letters 2024

doi: 10.1002/lol2.10376

LETTER

Vegetation promotes flow retardation and retention in deltaic wetlands

Xiaohe Zhang [1a]* *Cathleen E. Jones* [2] *Marc Simard* [2] *Paola Passalacqua* [3,4] *Talib Oliver-Cabrera* [2] *Sergio Fagherazzi* [1]

[1]Department of Earth and Environment, Boston University, Boston, Massachusetts, USA; [2]Jet Propulsion Laboratory, California Institute of Technology, Pasadena, California, USA; [3]Maseeh Department of Civil, Architectural and Environmental Engineering, The University of Texas, Austin, Texas, USA; [4]Department of Earth and Planetary Sciences, The University of Texas at Austin, Texas, USA

Scientific Significance Statement

The vegetation of coastal wetlands can dampen and delay incoming tides, affecting residence time and fluxes of nutrients and sediments. In the Wax Lake Delta, Louisiana, USA, we find that vegetation species like *Nelumbo lutea* colonizing the transition zone between submerged and emergent areas act as ecosystem engineers, creating more suitable hydrodynamic conditions for themselves. This natural vegetation front delays the ebb tide, augments the minimum water level inside the deltaic islands, and increases hydro-periods, thus creating better conditions for wetland species colonizing low elevations. This positive feedback between vegetation and hydraulics demonstrates the self-organization functionality of vegetation in deltaic stability.

Abstract

We introduce a new approach to observe the impact of vegetation on tidal flow retardation and retention at large spatial scales. Using radar interferometry and in situ water level gauge measurements during low tide, we find that vegetation in deltaic intertidal zones of the Wax Lake Delta, Louisiana, causes significant tidal distortion with both a delay (between 80 and 140 min) and amplitude reduction (~ 20 cm). The natural vegetation front delays the ebb tide, which increases the minimum water level and hydro-period inside the deltaic islands, resulting in better conditions for wetland species colonizing low elevations. This positive feedback between vegetation and hydraulics demonstrates the self-organization functionality of vegetation in the geomorphological evolution of deltas, which contributes to deltaic stability.

Coastal wetlands are widely recognized as sustainable and valuable natural barriers to destructive waves and flooding, with an average economic value of ~ \$1.8 million km^{-2} across the U.S. coast alone (Temmerman et al. 2013; Woodruff et al. 2013; Sun and Carson 2020). Wetland plants can naturally attenuate waves, reduce flow velocity, and accumulate sediments (Nepf

*Correspondence: zhangbu@bu.edu

[a]Present address: Institute of Estuarine and Coastal Research, School of Ocean Engineering and Technology, Sun Yat-Sen University, Guangzhou, China

Associate editor: Stephen Monismith

Author Contributions Statement: XZ analyzed the data and wrote the manuscript with support from SF, CJ, and MS helped supervise the project. XZ and SF conceived the original idea. CJ and TOC processed the UAVSAR data and provided the UAVSAR data. PP provided critical feedback for writing and figures. All the authors work for the National Aeronautics and Space Administration (NASA) Delta-X Mission.

Data Availability Statement: Data are available in the GitHub repository at https://github.com/BUxiaohezhang/WLD_flowdata/.

Additional Supporting Information may be found in the online version of this article.

and Vivoni 2000; Fagherazzi et al. 2012). However, the extent to which vegetation promotes adaptation to sea-level rise is unknown (Chadwick et al. 2022; Saintilan et al. 2022). Understanding the feedback between vegetation and hydrodynamics across the coastal landscape is, therefore, a scientific priority.

Previous work has mainly focused on the role of vegetation in attenuation of waves and peak water levels during storms (Möller et al. 2014; Stark et al. 2015; Montgomery et al. 2019; Temmerman et al. 2023). Only a few studies have addressed the effects of vegetation on ponding time and water storage at a large spatial scale (Montgomery et al. 2019). Numerical models show that vegetation induces flow attenuation and that a phase shift can affect water depth and inundation time and extent, further promoting the establishment and survival of vegetation (Rodríguez et al. 2017). In the Wax Lake Delta, Louisiana, USA, it is known that vegetation controls the hydrological connectivity of channels and islands (Hiatt and Passalacqua 2017; Sendrowski and Passalacqua 2017). However, sparse point measurements cannot capture spatial variations in tidal propagation over complex terrains like coastal marshes and swamps, and large-scale direct observations to estimate flow retardation and retention in these systems are needed.

Repeat-pass synthetic-aperture radar (SAR) interferometry (InSAR) enables measurements of water level changes within vegetation canopies (Lu and Kwoun 2008). The method relies on the fact that double bounce scattering of radar microwaves between water and vegetation results in a measurable phase shift between two measurements that is proportional to the water surface elevation change (Alsdorf et al. 2000; Lee et al. 2020). This spaceborne methodology has limited applicability in coastal areas due to the long revisit orbital period (days) compared to the duration of a tidal cycle (Wdowinski

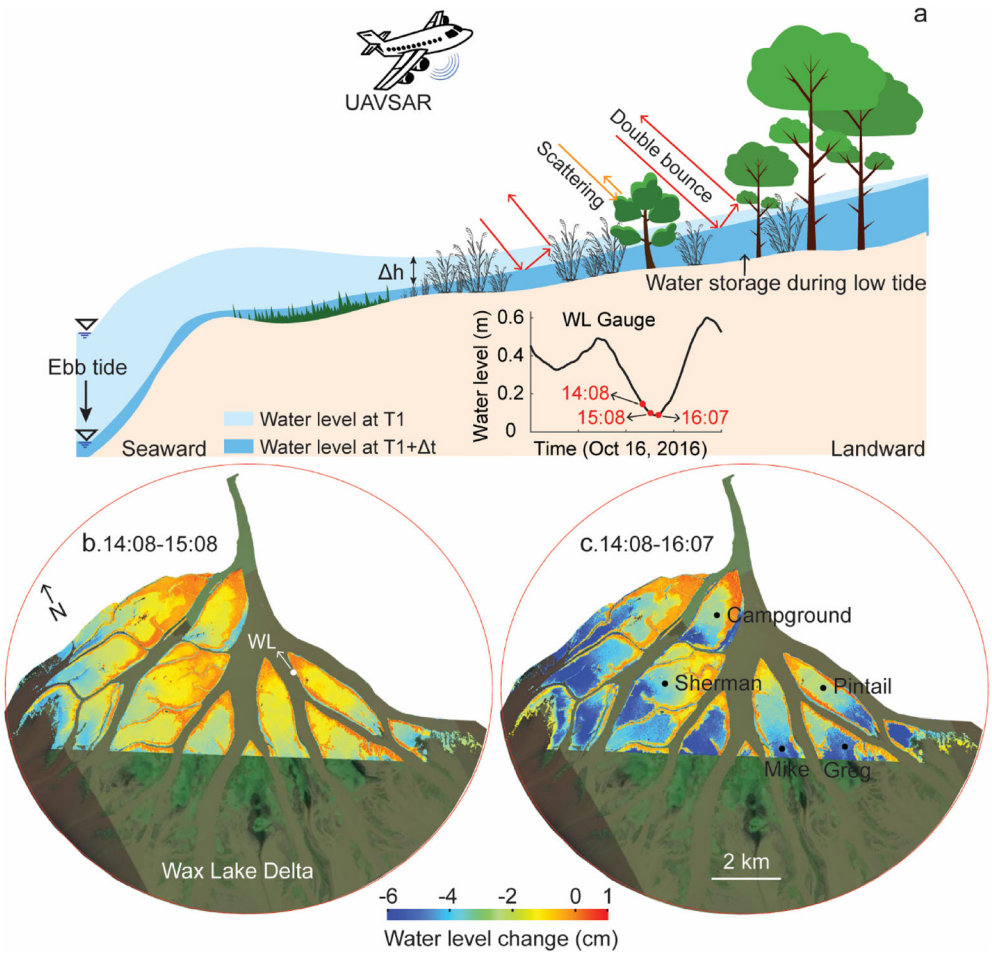

Fig. 1. Sub-canopy water level change measured by the uninhabited aerial vehicle synthetic-aperture radar (UAVSAR). (**a**) Schematic map of UAVSAR campaigns during the ebb tide and the double bounce radar scattering effects. InSAR was used to measure the change in water surface elevation, Δh, between times $T1$ and $T1 + \Delta t$ for each pixel in the scene. The tidal phase delay between channels and wetlands caused by vegetation friction leads to flow retention within wetlands. (**b**, **c**) Water surface elevation changes from 14:08 h to 15:08 h (**b**), and from 14:08 h to 16:07 h (**c**) on 16 October 2016 (GMT), during low tides in the Wax Lake Delta, Louisiana, USA (29.52°N, 91.44°W). The WL gauge recorded water level data (NAVD 88) in the same period.

et al. 2013; Liao et al. 2020). However, the use of an airborne instrument can shorten the repeat time interval to tens of minutes or hours, thereby directly measuring water level changes induced by tidal propagation during a single tidal cycle (Oliver-Cabrera et al. 2021; Zhang et al. 2022).

Here, we develop an empirical model linking water level changes to tidal delay and minimum water level based on field observations. These algorithms are then applied to water level change datasets from the uninhabited aerial vehicle SAR (UAVSAR) instrument, solving for the time delay and tidal distortion amplitude at low tide across the Wax Lake Delta. The high-resolution spatial dataset (10 m) of flow retardation and water retention, together with data on elevation and vegetation distribution, enable us to explore the interactions between vegetation, morphology, and hydrodynamics at a large spatial scale and at high resolution.

Materials and methods

The Wax Lake Delta is a naturally prograding river delta located in Atchafalaya Bay within the greater Mississippi River Delta. The Atchafalaya River distributes water and sediment into Atchafalaya Bay through the Wax Lake Outlet, which was dredged in 1942. Over time, the river formed a low-lying delta with distributary islands and channels (Shaw et al. 2013). The water level is modulated by a mixed semidiurnal micro-tide with a mean tidal range of up to 0.4 m. The average annual river discharge varies seasonally from 2500 to 5000 $m^3 s^{-1}$. The dominant vegetation species are the *Salix nigra* tree in the island highlands, the *Colocasia esculenta*, *Polygonum punctatum*, *Nelumbo lutea*, grasses, floating vegetation, and submerged aquatic vegetation in the intertidal zones (Carle et al. 2015; Ma et al. 2018; Jensen et al. 2019; *see* classification map in Supporting Information Fig. S2).

UAVSAR is a fully polarimetric (quad-polarization) L-band (wavelength $\lambda = 0.2379$ m, frequency $\nu = 1.257$ GHz) SAR operated by the U.S. National Aeronautics and Space Administration (NASA) and is deployed on a Gulfstream-3 aircraft (Fore et al. 2015). In this paper, we use UAVSAR data products representing water level changes during low tides collected between 14:08 h to 16:38 h on 16 October 2016 (Fig. 1) (Jones et al. 2021), and concurrent water level observations at a tidal gauge (WL site) installed in the Pintail channel (Fig. 2). InSAR-derived data of water level change and tide-gauge comparison show the error could be as low as 0.67 cm if carefully processed (Oliver-Cabrera et al. 2021). Time series UAVSAR data of water level change measured at 30-min intervals over the 2.5-h period are collected for validation of tidal time delay results (Fig. 4). Water surface elevation change with millimeter accuracy at the WL site was recorded every 5 min using in situ pressure transducers during the NASA Pre-Delta-X Campaign on 13 October 2016–20 October 2016 (Simard et al. 2020).

Since we do not have water level measurements in vegetated surfaces in 2016, we use data obtained from loggers

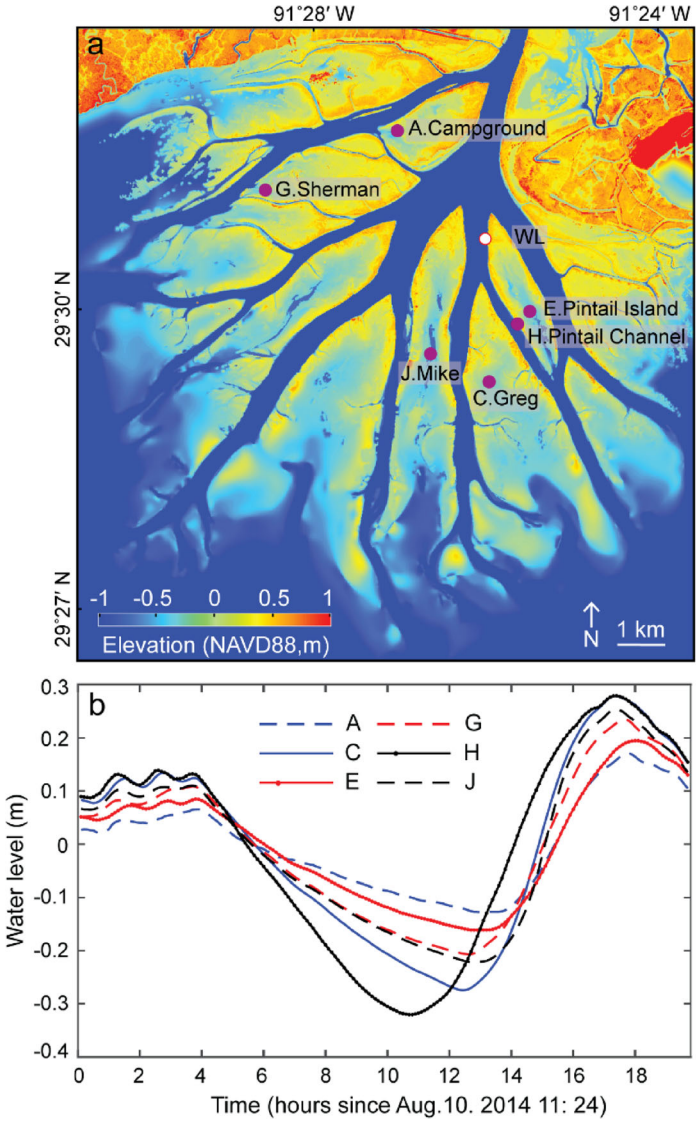

Fig. 2. Field measurements of water level. (**a**) Locations of field sites (A, C, E, G, H, J) where tidal gauges were located in 2014 (Sendrowski and Passalacqua 2017) and WL gauge in 2016, plotted on top of the DEM. (**b**) Water levels relative to the mean tidal water levels in 2014.

installed on five islands (Fig. 2) and one in the Pintail channel (H site) in August 2014 (Sendrowski and Passalacqua 2017). The river discharge during August 2014 is comparable to the UAVSAR campaign in 2016. Since the 2014 water level data are not vertically georeferenced, we calculate the water level relative to the mean water level in tidal cycles at each site.

We select the tidal cycle in 2014 during which the water elevations at site H are closest to the signal at site WL in 2016 (Pintail channel). The comparison of water elevations in 2014 and 2016 yields an $R^2 = 0.995$ and RMSE = 0.011 m (Supporting Information Fig. S1). We, therefore, assume that the water levels in the vegetated areas of the islands during

the selected tidal cycle in 2014 are very similar to the water levels during the 2016 UAVSAR campaign.

The topography used in this analysis is a 10-m seamless digital elevation model (DEM) composed of LiDAR datasets and sonar transects in channels referred to the NAVD88 vertical datum (Denbina et al. 2020). We calculate the normalized difference vegetation index (NDVI) during the vegetation peak season, using Sentinel-2 imagery taken on 13 October 2016. NDVI is a proxy for vegetation abundance with values ranging from 0 to 1. Maps of vegetation species and biomass (Byrd et al. 2018; Jensen et al. 2021) are also utilized to understand the role of vegetation on tidal propagation (Supporting Information Fig. S3).

Since UAVSAR data are collected during low tides, a higher value of water level change implies a fast drop in water level, resulting in a small tidal time delay and a lower minimum water level (Fig. 2b). Therefore, we use the tidal signals measured at few gauges and concurrent UAVSAR data to derive the large-scale spatial distribution of hydrodynamic parameters. We are particularly interested in the tidal signal delay between the channel and island vegetation and in the minimum water level during the tidal cycle, which is a proxy for water storage in the vegetated area. Specifically, time delays of low tidal signals at five gauges on different islands (A, C, E, G, J in Fig. 2) relative to one gauge in channel water (H) are calculated to build the regression model between time delay and water level change (Fig. 3a). Similarly, the regression model between minimum water levels and water level changes is built based on data of five gauges on the islands (Fig. 3d).

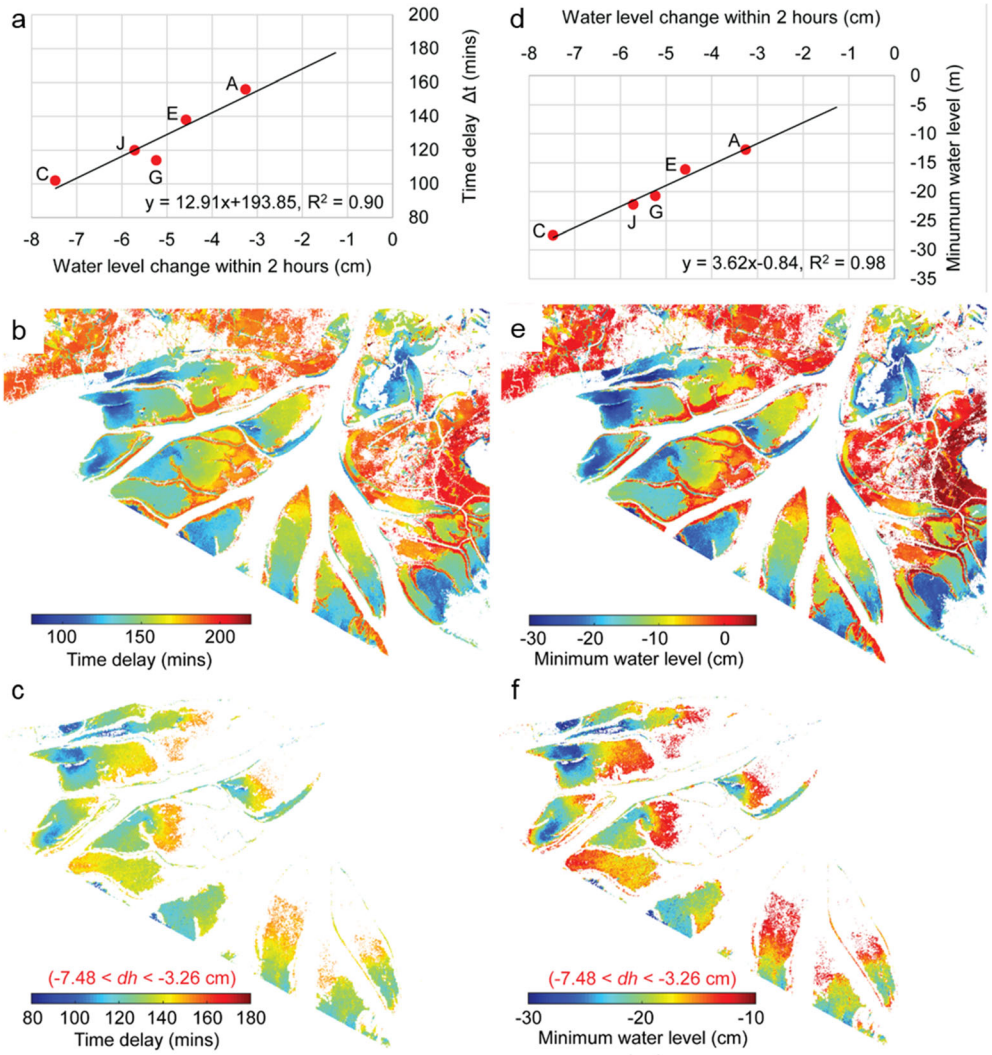

Fig. 3. Spatial maps of tidal time delay and minimum water level. (**a**) Time delay and (**d**) minimum water level as a function of water level change observed at locations indicated in Fig. 2, (**b**) time delay computed using the relationship in (**a**), and (**e**) derived minimum water levels computed using the relationship in (**d**); (**c**) time delay and (**f**) minimum water level only within the range -7.48 cm $< dh < -3.26$ cm. *dh* indicates water level change within 2 h (Fig. 1c).

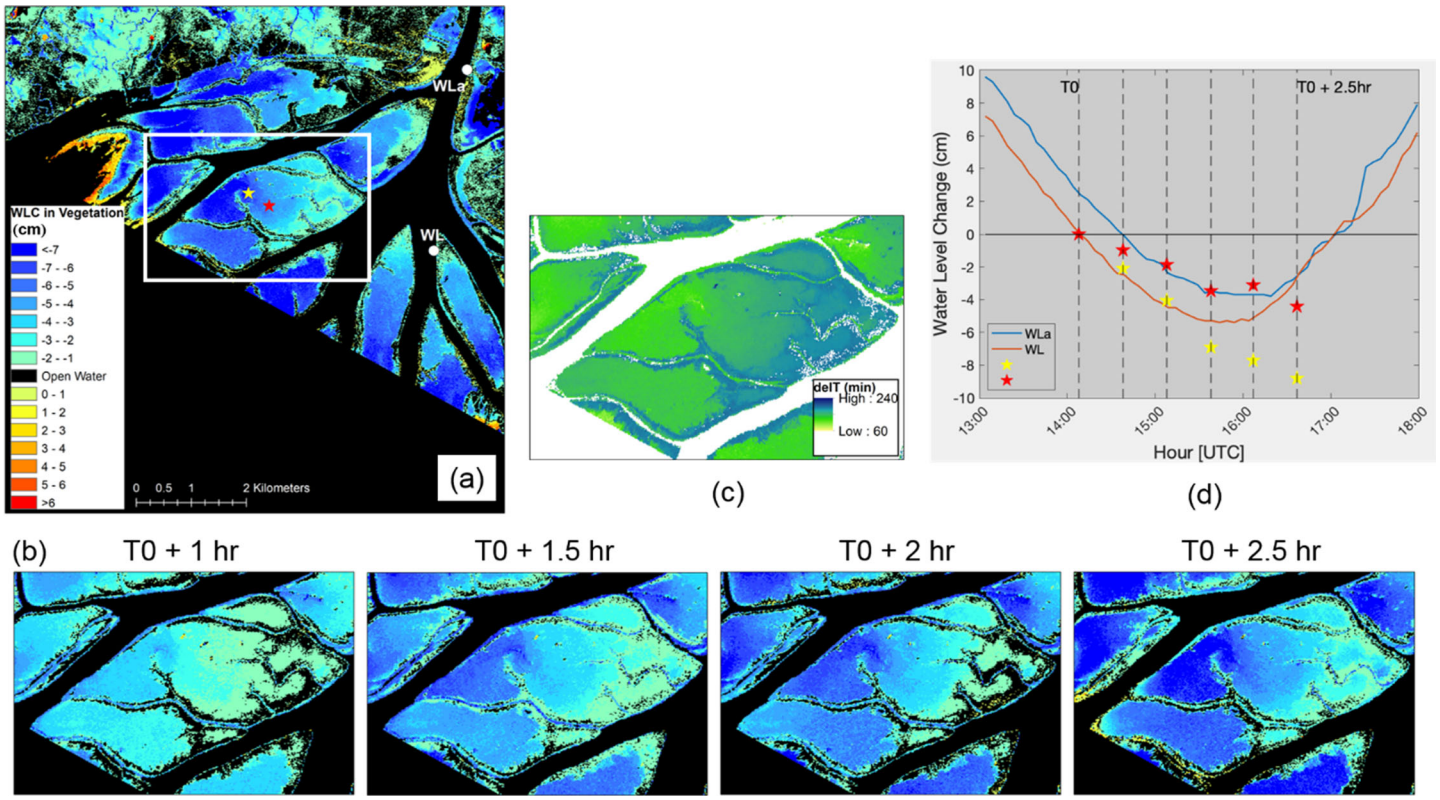

Fig. 4. Measured water level change (WLC) vs. time. (**a**) Cumulative water level change over the 2.5-h period on 16 October 2016, measured by UAVSAR using InSAR. The white circles show the locations of two in-channel water level gauges that provide concurrent measurements with the UAVSAR collections. (**b**) Time series of water level change measured at 30-min intervals over the 2.5-h period for the area outlined in (**a**). (**c**) Tidal time delay from the model for the region shown in (**b**). The patterns of delay follow the patterns of water level change shown in (**b**). (**d**) Water level change for the water gauges and interior island locations (denoted by stars in (**a**)), all referenced to the water level at the time of the first UAVSAR acquisition (T0). The minima measured by gauge WL occurs around time T0 + 1.5 h. The water levels at the two inland locations are still decreasing at the time of the last acquisition, 1 h later. The model shows minima in the island interior occurring from 1 to 3 h after the minima at WL, with the earlier minima occurring at the same locations that the UAVSAR data show rapid water level change.

These two models are then applied to UAVSAR data to derive the spatial distribution of tidal time delay and minimum water level (Fig. 3b,e).

We use several methods to control the quality and accuracy of model results. First, because the reference gauge is located in a deltaic channel, the regression models are only valid for the flow exchange between channels and islands. Results at the island tails where tidal flows are coming from the ocean should be excluded (*see* red colors in Fig. 4a). Second, we further limit the results within the range of water level change dh detected by UAVSAR ($-7.48 < dh < -3.26$ cm within the $\sim$ 2 h observed by UAVSAR) and assume the regression results outside of this range are less accurate. While UAVSAR can detect dh in a range of around 10 cm (Fig. 4a), the limited range of $-7.48 < dh < -3.26$ cm based on the tidal signal at five gauges used for the regression analysis can increase accuracy. Finally, the regression model is only valid during the ebb tide and not for the turning of the tidal signal (Fig. 4a). Therefore, the regression between UAVSAR and gauges is limited to the ebb tide between 14:08 h and 16:07 h, before the beginning of the flood phase (Fig. 1).

To validate model results, we use time series data of UAVSAR at $\sim$ 30-min intervals at two locations on Sherman Island (Fig. 4). The water levels at these locations are still decreasing at the time of the last acquisition, while the water levels in the channel are already increasing after reaching the lowest water level. At these locations, we can, therefore, compute the time delay directly from the UAVSAR time series and use it to validate the model results.

Results

The UAVSAR measurements show a large gradient in water level change within deltaic islands (Fig. 1). The water level drops about 6 cm seaward along the 3.5 km-long Pintail Island within a 2-h window during the low ebb tide (Fig. 1). The gradients imply a large change in amplitude and time delay of the tide during its propagation within the island.

Relatively small water level changes in the uplands of Sherman Island and along the margins of secondary channels are probably due to high elevations and the presence of high-land vegetation species (e.g., *S. nigra*) that reduce flow connectivity. Because the water level in the islands' interior drops less than at the islands' margins and adjacent channels, water retained in the islands' interior fails to discharge into the ocean before the next incoming tide floods the island. As a result, a portion of the tidal volume is stored in the islands during low tide (Fig. 1; Montgomery et al. 2019).

The time delay of the minimum water level is linearly correlated to the 2-h water level change (Fig. 3a, $y = 12.91x + 193.85$, $R^2 = 0.90$, $p < 0.001$). The calculated time delay generally increases from the island tail to the head, while in Campground Island, it increases eastward following the elevation gradient (Fig. 3b). The time delay is between 80 and 140 min in most areas of the islands (Fig. 3c). The results indicate a sharp time delay at low tide in the islands tail relative to the signal in the channel, with a delay of 100 min at the island margin. The modeled time delay agrees well with the delay directly computed from the time series of UAVSAR data of water level change (Supporting Information Fig. S2b,c). As locations in Sherman Island have not reached the minimum water level during the UAVSAR campaign, the time delay is at least 1 h with respect to the channel gauge (Supporting Information Fig. S2d).

The low water levels are also linearly correlated to the 2-h water level changes (Fig. 3d, $y = 3.62x - 0.84$, $R^2 = 0.98$, $p < 0.001$). The difference in low water levels from the island to the channel banks is up to 40 cm, with a large spatial variability (Fig. 3e). We find that most of the phase shift and attenuation of the tidal range occurs during low tide rather than high tide (Fig. 2b), which highlights the importance of tidal distortion during low water levels in modulating tidal propagation.

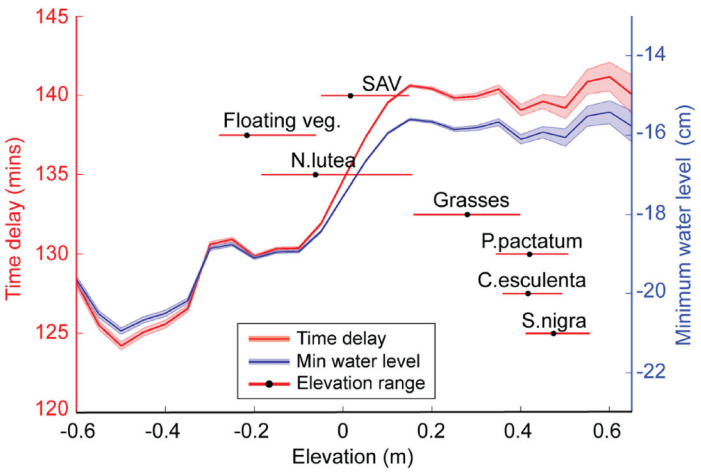

Fig. 5. Role of vegetation on tidal delay and water retention. Minimum water level and time delay (data from Fig. 3c,f, respectively) as a function of elevation (NAVD 88). Elevation range of dominant vegetation species (red line, 25th percentile, mean and 75th percentile values). Data are shown with 1σ confidence intervals binned by 0.05 m of elevation. SAV represents submerged aquatic vegetation (Jensen et al. 2021).

To understand the influence of topography and vegetation on hydrodynamics, we compute the time delay of the low tide and lowest water level as a function of elevation and dominant vegetation species (Fig. 5). We limit the calculation to 2-h water level changes ranging from −7.48 to −3.26 cm (Figs. 2a, 3c,f). We find that the delay in tidal propagation and minimum water level generally increases with elevation, but a sharp increase occurs at intermediate elevations ranging from −0.1 to 0.15 m. The average time delay increases by about 11 min and the minimum water level increases by about 4 cm within this 0.25 m elevation range (Fig. 5).

This elevation range is characterized by the dominant vegetation species *N. lutea*, which covers more than 50% of the island area (Supporting Information Fig. S2). This intermediate elevation range is characterized by higher NDVI and vegetation biomass values relative to the island highlands (Supporting Information Fig. S3). The margin of *N. lutea* (*see* class 5 in Supporting Information Fig. S2) exerts a strong control on flow retardation and retention, while elevation is of secondary importance and has a stronger effect on tidal distortion outside this vegetated strip (Supporting Information Fig. S4). For unvegetated areas with elevations between −0.6 and −0.2 m, the elevation-averaged tidal phase delay is about 5 min. The delay time doubles to 10 min in vegetated areas with elevation between −0.2 and 0.15 m (Fig. 5), highlighting the role of vegetation in delaying the flow.

Our results show potential evidence that *N. lutea* encroachment at intermediate elevations engineers the interior of the islands to retain more water and reduce tidal range. The vegetation delays the ebb tide, increases the minimum water level inside the islands, creating deeper water, and longer hydroperiods. Long hydro-periods prevent the encroachment of less flood-resistant vegetation that would outcompete *N. lutea*. *N. lutea* can thus spread in topographically higher areas, facing less competition, further increasing water retention and tidal delay in positive feedback. Since the delta experienced in recent years a significant expansion of *N. lutea* with an encroachment rate of 2.7 $km^2\ yr^{-1}$ (Jensen et al. 2021), this positive feedback between vegetation and hydraulics might showcase the self-organization functionality of vegetation in the geomorphological evolution of deltas.

Discussion

While previous work regarding the effects of vegetation on coastal wetland hydrodynamics mainly focused on the attenuation of waves and flooding peak water levels (Möller et al. 2014; Stark et al. 2015), we introduced a new method to quantify at high spatial resolution vegetation-induced water storage at low tide. This method is based on a combination of

airborne rapid repeat InSAR technique, field observations of water levels, LiDAR-derived topography, and vegetation index derived from optical satellite imagery. Our results demonstrate that deltaic island vegetation causes significant tidal distortion with both a delay (between 80 and 140 min in most areas) and amplitude reduction (~ 20 cm) during low tide. The large spatial gradients of time delay and low water levels calculated over the wetlands clearly illustrate the location where water ponding is more pronounced (higher water storage during low tide).

We demonstrate that sub-canopy water level changes detected by repeat-pass interferometry can be used to derive information on both tidal propagation delay and minimum water level during low tides. Current spaceborne radar images with a repeat time interval of a few days to weeks cannot capture the hydrodynamics during one tidal cycle and can only provide information on long-term hydrological processes in coastal wetlands (e.g., river discharge and neap-spring tides; Liao et al. 2020). Future spaceborne missions with a shorter repeat time interval would offer a cost-effective and efficient way to acquire tidal hydrodynamic data across more coastal wetlands.

The water storage effect highlighted by our data changes inundation depth and hydroperiod, likely affecting residence time and nutrient removal (Knights et al. 2020), carbon sequestration (Shields et al. 2017), sediment deposition (Nardin and Edmonds 2014), and vegetation zonation (Day et al. 2006). For example, Knights et al. (2020) found that intermediate elevation areas in the Wax Lake Delta, corresponding to the ones identified here (Fig. 5), are hot spots for nitrate removal. This effect might be enhanced if a large fraction of tidal water is stored in a tidal cycle, thus increasing residence time. The rising sea level worldwide would further complicate these ecological and hydrodynamic functionalities, for example, stronger saltwater intrusion, longer flow residence time, and more water storage could substantially modify the vegetation zonation patterns (Kirwan and Gedan 2019). Therefore, high spatial–temporal data of water quality from spaceborne and airborne sensors should also be involved in future research to better understand the ecological and morphological evolution of wetland systems.

In river deltas like Wax Lake Delta, the water surface elevation in the channel is often higher than in the island. As a result, a significant amount of lateral outflow (23–54% of discharge) debouches into the island wetlands even at low river discharge (Hiatt and Passalacqua 2015). Therefore, detailed analyses of wetland hydrodynamics are necessary to quantitatively evaluate the critical role of deltaic wetlands in regulating flow discharge, tidal propagation, and sedimentation. The results demonstrate the successful implementation of UAVSAR and derived tidal hydrodynamics in a microtidal system with multiple vegetation species. We expect that in other tidal systems with large tidal signals, the significant sub-canopy water level changes could be more easily detected, allowing us to better capture the spatially varying hydrodynamics of coastal wetlands. On the contrary, in deltaic wetlands with very short vegetation or where the vegetation is completely submerged or always emergent UAVSAR would not provide meaningful data. Deltas with large, vegetated areas that undergo wetting and drying would also be amenable to this method.

Our novel methodology provides a promising way to quantify the interactions between vegetation and hydrodynamics over large areas, with potential applications in other coastal wetlands around the globe.

References

Alsdorf, D., J. Melack, T. Dunne, L. A. Mertes, L. L. Hess, and L. C. Smith. 2000. Interferometric radar measurements of water level changes on the Amazon flood plain. Nature **404**: 174–177. doi:10.1038/35004560

Byrd, K. B., L. Ballanti, N. Thomas, D. Nguyen, J. R. Holmquist, M. Simard, and L. Windham-Myers. 2018. A remote sensing-based model of tidal marsh aboveground carbon stocks for the conterminous United States. ISPRS J. Photogramm. Remote Sens. **139**: 255–271. doi:10.1016/j.isprsjprs.2018.03.019

Carle, M. V., C. E. Sasser, and H. H. Roberts. 2015. Accretion and vegetation community change in the Wax Lake Delta following the historic 2011 Mississippi River flood. J. Coast. Res. **31**: 569–587. doi:10.2112/JCOASTRES-D-13-00109.1

Chadwick, A. J., S. Steele, J. Silvestre, and M. P. Lamb. 2022. More extensive land loss expected on coastal deltas due to rivers jumping course during sea-level rise. Proc. Natl. Acad. Sci. USA **119**: e2119333119. doi:10.1073/pnas.2119333119

Day, R. H., T. W. Doyle, and R. O. Draugelis-Dale. 2006. Interactive effects of substrate, hydroperiod, and nutrients on seedling growth of *Salix nigra* and *Taxodium distichum*. Environ. Exp. Bot. **55**: 163–174. doi:10.1016/j.envexpbot.2004.10.009

Denbina, M. W., M. Simard, T. M. Pavelsky, A. I. Christensen, K. Liu, and C. Lyon. 2020. Pre-Delta-X: Channel bathymetry of the Atchafalaya Basin, LA, USA, 2016. ORNL DAAC. doi:10.3334/ORNLDAAC/1807

Fagherazzi, S., and others. 2012. Numerical models of salt marsh evolution: Ecological, geomorphic, and climatic factors. Rev. Geophys. **50**. doi:10.1029/2011RG000359

Fore, A. G., B. D. Chapman, B. P. Hawkins, S. Hensley, C. E. Jones, T. R. Michel, and R. J. Muellerschoen. 2015. UAVSAR polarimetric calibration. IEEE Trans. Geosci. Remote Sens. **53**: 3481–3491. doi:10.1109/TGRS.2014.2377637

Hiatt, M., and P. Passalacqua. 2015. Hydrological connectivity in river deltas: The first-order importance of channel-island exchange. Water Resour. Res. **51**: 2264–2282. doi:10.1002/2014WR016149

Hiatt, M., and P. Passalacqua. 2017. What controls the transition from confined to unconfined flow? Analysis of

hydraulics in a coastal river delta. J. Hydraul. Eng. **143**: 03117003. doi:10.1061/(ASCE)HY.1943-7900.0001309

Jensen, D., K. C. Cavanaugh, M. Simard, G. S. Okin, E. Castañeda-Moya, A. McCall, and R. R. Twilley. 2019. Integrating imaging spectrometer and synthetic aperture radar data for estimating wetland vegetation aboveground biomass in coastal Louisiana. Remote Sens. **11**: 2533. doi:10.3390/rs11212533

Jensen, D., K. C. Cavanaugh, M. Simard, A. Christensen, A. Rovai, and R. Twilley. 2021. Aboveground biomass distributions and vegetation composition changes in Louisiana's Wax Lake Delta. Estuar. Coast. Shelf Sci. **250**: 107139. doi:10.1016/j.ecss.2020.107139

Jones, C., M. Simard, and Y. Lou. 2021. Pre-Delta-X: UAVSAR-derived water level change maps, Atchafalaya Basin, LA, USA, 2016. ORNL DAAC. doi:10.3334/ORNLDAAC/1823

Kirwan, M. L., and K. B. Gedan. 2019. Sea-level driven land conversion and the formation of ghost forests. Nat. Clim. Change **9**: 450–457. doi:10.1038/s41558-019-0488-7

Knights, D., A. H. Sawyer, R. T. Barnes, A. Piliouras, J. Schwenk, D. A. Edmonds, and A. M. Brown. 2020. Nitrate removal across ecogeomorphic zones in Wax Lake Delta, Louisiana (USA). Water Resour. Res. **56**: e2019WR026867. doi:10.1029/2019WR026867

Lee, H., T. Yuan, H. Yu, and H. C. Jung. 2020. Interferometric SAR for wetland hydrology: An overview of methods, challenges, and trends. IEEE Geosci. Remote Sens. Mag. **8**: 120–135. doi:10.1109/MGRS.2019.2958653

Liao, T. H., M. Simard, M. Denbina, and M. P. Lamb. 2020. Monitoring water level change and seasonal vegetation change in the coastal wetlands of louisiana using L-band time-series. Remote Sens. **12**: 2351. doi:10.3390/rs12152351

Lu, Z., and O. I. Kwoun. 2008. Radarsat-1 and ERS InSAR analysis over southeastern coastal Louisiana: Implications for mapping water-level changes beneath swamp forests. IEEE Trans. Geosci. Remote Sens. **46**: 2167–2184. doi:10.1109/TGRS.2008.917271

Ma, H., L. G. Larsen, and R. W. Wagner. 2018. Ecogeomorphic feedbacks that grow deltas. J. Geophys. Res.: Earth Surf. **123**: 3228–3250. doi:10.1029/2018JF004706

Möller, I., and others. 2014. Wave attenuation over coastal salt marshes under storm surge conditions. Nat. Geosci. **7**: 727–731. doi:10.1038/ngeo2251

Montgomery, J. M., K. R. Bryan, J. C. Mullarney, and E. M. Horstman. 2019. Attenuation of storm surges by coastal mangroves. Geophys. Res. Lett. **46**: 2680–2689. doi:10.1029/2018GL081636

Nardin, W., and D. Edmonds. 2014. Optimum vegetation height and density for inorganic sedimentation in deltaic marshes. Nat. Geosci. **7**: 722–726. doi:10.1038/ngeo2233

Nepf, H. M., and E. R. Vivoni. 2000. Flow structure in depth-limited, vegetated flow. J. Geophys. Res.: Oceans **105**: 28547–28557. doi:10.1029/2000JC900145

Oliver-Cabrera, T., C. E. Jones, Z. Yunjun, and M. Simard. 2021. InSAR phase unwrapping error correction for rapid repeat measurements of water level change in wetlands. IEEE Trans. Geosci. Remote Sens. **60**: 5215115. doi:10.1109/TGRS.2021.3108751

Rodríguez, J., P. Saco, S. Sandi, N. Saintilan, and G. Riccardi. 2017. Potential increase in coastal wetland vulnerability to sea-level rise suggested by considering hydrodynamic attenuation effects. Nat. Commun. **8**: 16094. doi:10.1038/ncomms16094

Saintilan, N., and others. 2022. Constraints on the adjustment of tidal marshes to accelerating sea level rise. Science **377**: 523–527. doi:10.1126/science.abo7872

Sendrowski, A., and P. Passalacqua. 2017. Process connectivity in a naturally prograding river delta. Water Resour. Res. **53**: 1841–1863. doi:10.1002/2016WR019768

Shaw, J. B., D. Mohrig, and S. K. Whitman. 2013. The morphology and evolution of channels on the Wax Lake Delta, Louisiana, USA. J. Geophys. Res.: Earth Surf. **118**: 1562–1584. doi:10.1002/jgrf.20123

Shields, M., T. Bianchi, D. Mohrig, J. A. Hutchings, W. F. Kenney, A. S. Kolker, and J. H. Curtis. 2017. Carbon storage in the Mississippi River delta enhanced by environmental engineering. Nat. Geosci. **10**: 846–851. doi:10.1038/ngeo3044

Simard, M., M. W. Denbina, D. J. Jensen, and R. Lane. 2020. Pre-Delta-X: Water levels across Wax Lake Outlet, Atchafalaya Basin, LA, USA, 2016. ORNL DAAC. doi:10.3334/ORNLDAAC/1801

Stark, J., T. van Oyen, P. Meire, and S. Temmerman. 2015. Observations of tidal and storm surge attenuation in a large tidal marsh. Limnol. Oceanogr. **60**: 1371–1381. doi:10.1002/lno.10104

Sun, F., and R. T. Carson. 2020. Coastal wetlands reduce property damage during tropical cyclones. Proc. Natl. Acad. Sci. USA **117**: 5719–5725. doi:10.1073/pnas.1915169117

Temmerman, S., P. Meire, T. Bouma, P. M. J. Herman, T. Ysebaert, and H. J. De Vriend. 2013. Ecosystem-based coastal defence in the face of global change. Nature **504**: 79–83. doi:10.1038/nature12859

Temmerman, S., E. M. Horstman, K. W. Krauss, J. C. Mullarney, I. Pelckmans, and K. Schoutens. 2023. Marshes and mangroves as nature-based coastal storm buffers. Ann. Rev. Mar. Sci. **15**: 95–118. doi:10.1146/annurev-marine-040422-092951

Wdowinski, S., S. H. Hong, A. Mulcan, and B. Brisco. 2013. Remote-sensing monitoring of tide propagation through coastal wetlands. Oceanography **26**: 64–69. doi:10.5670/oceanog.2013.46

Woodruff, J., J. Irish, and S. Camargo. 2013. Coastal flooding by tropical cyclones and sea-level rise. Nature **504**: 44–52. doi:10.1038/nature12855

Zhang, X., C. E. Jones, T. Oliver-Cabrera, M. Simard, and S. Fagherazzi. 2022. Using rapid repeat SAR interferometry to

improve hydrodynamic models of flood propagation in coastal wetlands. Adv. Water Resour. **159**: 104088. doi:10.1016/j.advwatres.2021.104088

Acknowledgments

This work (NASA Delta-X mission) was funded by the Science Mission Directorate's Earth Science Division through the Earth Venture Suborbital-3 Program NNH17ZDA001N-EVS3. This work was partly performed by the Jet Propulsion Laboratory, California Institute of Technology, under contract with the National Aeronautics and Space Administration (NASA). All the data are provided in the Supporting Information file. SF was also partially funded by NSF grants DEB-1832221 to the Virginia Coast Reserve Long-Term Ecological Research project and OCE-2224608 to the Plum Island Ecosystems Long-Term Ecological Research project.

Submitted 29 October 2023
Revised 10 January 2024
Accepted 15 January 2024